Measurement report: Fast photochemical production of peroxyacetyl nitrate (PAN) over the rural North China Plain during haze events in autumn

Yulu Qiu[1,2,3,4], Zhiqiang Ma[1,3,4,*], Ke Li[2], Mengyu Huang[5], Jiujiang Sheng[5], Ping Tian[5], Jia Zhu[2], Weiwei Pu[3,4], Yingxiao Tang[6], Tingting Han[3,4], Huaigang Zhou[3,4], and Hong Liao[2]

[1]Institute of Urban Meteorology, China Meteorological Administration, Beijing, 100089, China
[2]Collaborative Innovation Center of Atmospheric Environment and Equipment Technology, Jiangsu Key Laboratory of Atmospheric Environment Monitoring and Pollution Control (AEMPC), School of Environmental Science and Engineering, Nanjing University of Information Science & Technology, Nanjing, 210044, China
[3]Beijing Shangdianzi Regional Atmosphere Watch Station, Beijing, 101507, China
[4]Environmental Meteorology Forecast Center of Beijing-Tianjin-Hebei, Beijing, 100089, China
[5]Beijing Weather Modification Office, Beijing, 100089, China
[6]Tianjin Environmental Meteorology Center, Tianjin, 300074, China

Correspondence to: Zhiqiang Ma (zqma@ium.cn)

Abstract. Photochemical pollution over the North China Plain (NCP) is attracting much concern. We usually view peroxyacetyl nitrate (PAN) as the second most important photochemical pollutant featuring high mixing ratios during warm seasons. Our observations at a background site in the NCP identified high PAN concentrations even during haze events in autumn. The substantial increasing ratios of PAN by 244% and 178% over the morning hours (8:00–12:00) on 10/20 and 10/25, 2020 were 10.6 and 7.7 times larger than those on clean days. We characterize the pollution days by higher temperature, higher humidity and anomalous southerly winds compared with clean days. Enhanced local photochemistry has been identified as the dominant factor that controls PAN increase in the morning at the rural site, as the time when prevailing wind turns to southerly wind is too late to promote direct transport of PAN from the polluted urban region. By removing the effect of direct transport of PAN, we provide a quantitative assessment of net PAN chemical production rate of 0.45 ppb h^{-1} on the morning of pollution days, also demonstrating the strong local photochemistry. Using observations and calculated photolysis rates, we find that acetaldehyde oxidation by hydroxyl radical (OH) is the primary pathway of peroxyacetyl radical formation at the rural site. Acetaldehyde concentrations and production rates of HO$_x$ (HO$_x$ = OH + HO$_2$) on pollution days are 2.8 and 2 times as large as those on clean days, leading to remarkable increase of PAN in the morning. Formaldehyde (HCHO) photolysis dominates the daytime HO$_x$ production, thus contributing to fast photochemistry of PAN. Our observational results suggest the cause of rapid increase of PAN during haze events in autumn at a rural site of the NCP, also provide the evidence of important role of HCHO photolysis in secondary pollutants at lower nitrogen oxide emissions. This highlights the urgent to carry out strict volatile organic compounds controls out of summer seasons over the NCP.

1 Introduction

Since the late 1960s, peroxyacetyl nitrate (PAN) has been identified as a key photochemical pollutant in the atmosphere, having adverse effects in human health and vegetation (Heuss and Glasson, 1968; Taylor, 1969). It is a secondary pollutant formed through reactions between peroxyacetyl radical ($CH_3C(O)O_2$, PA) and nitrogen dioxide (NO_2) (Xue et al., 2014). The dominant three pathways of PA formation are through oxidation of acetaldehyde (CH_3CHO), photolysis of acetone ($CH_3C(O)CH_3$) and methylglyoxal (CH_3COCHO, MGLY) (Fischer et al., 2014):

$$CH_3CHO + OH \xrightarrow{O_2} PA + H_2O \tag{R1}$$

$$CH_3C(O)CH_3 + hv \xrightarrow{O_2} PA + CH_3 \tag{R2}$$

$$CH_3COCHO + hv \xrightarrow{O_2} PA + HCO \tag{R3}$$

PAN can be thermally decomposed back to PA and NO_2 which is the major removal pathway in the lower troposphere:

$$PAN \leftrightarrow PA + NO_2 \tag{R4}$$

PAN's precursors, such as CH_3CHO, acetone and MGLY, are usually viewed as the second-generation precursors, because they not only directly come from anthropogenic emissions but also are oxidation products of various non-methane hydrocarbons (NMHCs) (Xue et al., 2014). These NMHCs are first-generation precursors. Thus, photochemical production of PAN could be largely determined by the oxidation of volatile organic compounds (VOCs) with radicals in the presence of nitrogen oxide ($NO_x = NO + NO_2$). During the daytime, hydroxyl (OH) radical is usually considered as the primary oxidant in the troposphere. Nitrous acid (HONO), mainly generated from direct traffic emissions and heterogeneous conversion of NO_2 on ground and aerosol surfaces (Xue et al., 2020; Liu et al., 2021), is a key source of OH radical in the early morning (Alicke et al., 2003) and during cold days (Hendrick et al., 2014; Kim et al., 2014; Lu et al., 2019). In addition, photolysis of carbonyls may also greatly influence HO_x ($HO_x = OH + HO_2$) and ozone (O_3) production at lower NO_x concentrations during cold seasons (Edwards et al., 2014; Li et al., 2021). For example, Li et al. (2021) found that HO_x radicals from photolysis of formaldehyde (HCHO) accelerated the ozone upsurge during COVID-19 in Beijing in response to substantial NO_x reductions.

The North China Plain (NCP) region is now experiencing urbanization and industrial expansions, leading to air pollution as a matter of intense debate. Since 2013, the China Government has performed strict emission reduction measures and resulted in rapid decrease of $PM_{2.5}$ concentration (Zhai et al., 2019). However, increases of O_3 concentrations in the NCP region have been frequently reported owing to large amounts of anthropogenic precursor emissions and meteorological variability so far (Ma et al., 2016; Li et al., 2020; Lu et al., 2020; Dang et al., 2021). Li et al. (2020) reported that the maximum 8h average (MDA8) O_3 concentrations in summer NCP during 2013−2019 were increased by a rate of 3.3 ppb a^{-1}. As another important photochemical pollutant, PAN pollution events were also extensively recognized both in the urban (Zhang et al., 2014; Zhang et al., 2015; Zhang et al., 2017; Qiu et al., 2019a) and rural NCP regions (Qiu et al., 2020a; Wei et al., 2020) at the same time. These also confirm the severity and complexity of photochemical pollution in this highly-populated NCP region.

Compared with the relatively low concentration of O_3 in autumn and winter seasons (Wang et al., 2013), PAN pollution events are also observed in cold days over the NCP (Zhang et al., 2014; Liu et al., 2018; Zhang et al., 2019; Zhang et al., 2020a; Qiu et al., 2019b; 2020b) associated with particulate pollution events. For example, Qiu et al. (2020b) reported a high PAN level of 4.13 ppb during the COVID-19 lockdown period of January–February 2020 in Beijing, and the average value was 52% higher than that in summer 2019 when solar radiation was intensive. A common explanation for the observed high PAN concentration in winter is its susceptibility to be accumulated under a stable atmosphere and regional transport due to decreased thermal decomposition under low temperatures (Qiu et al., 2019b; Zhang et al., 2020a). Besides, accelerated photochemistry can also play a role during PAN pollution events in cold days (Zhang et al., 2014; Liu et al., 2018; Qiu et al., 2020b; Zhang et al., 2020a) since unexpectedly high PAN concentrations are usually observed during the daytime. Thus, PAN could represent a key indicator of photochemistry in cold days.

Despite several field campaigns and experiment analysis in recent years, the fast PAN formation mechanisms during autumn and winter over the NCP region still have not been fully explored so far, especially over clean rural regions. Previously, HONO photolysis was tentatively considered as the cause of strengthened local photochemistry in winter of urban NCP region, thus contributing to increases in PAN concentrations (Liu et al., 2018; Zhang et al., 2020b). For example, Liu et al. (2018) found a positive relationship between HONO and PAN in winter over an urban site of the NCP, thus highlighted the importance of HONO in faster PAN formation during haze episodes. By conducting sensitivity simulations using the WRF-Chem model, Zhang et al. (2020b) reported that HONO photolysis could result in 80%–150% PAN increases in eastern China during pollution days in winter. However, these studies neglect the impact of carbonyl photolysis that allows for fast photochemistry and may play a dominant role in PAN formation over the rural region with low NO_x emissions. The lack of integrated observation of VOCs, HONO and other related chemical species in previous studies hinders the comprehensive understanding of PAN chemistry.

Here, we first show observational evidence of fast PAN formation at a rural site of the NCP during haze events in autumn 2020. The dominant contribution from enhanced local photochemistry to PAN concentration increases is verified by analysis between variations in wind and PAN concentrations, along with quantitative assessment of direct physical transport utilizing carbon monoxide (CO) as a tracer. Using simultaneous observations of PAN, VOCs, HONO, and photolysis rates, we calculate the daytime HO_x production rates and reveal the contributions of precursors and radical oxidants in daytime PAN increases. Our results suggest the cause of rapid PAN increase over the rural NCP, and provide a new insight into assessing impacts of high reactive VOCs from urban plumes on atmospheric oxidation capacity and secondary pollutant formation over the rural NCP.

2 Experiments and Methods

2.1 Site

We conduct the field campaign at the Shangdianzi (SDZ) national atmospheric background station, which is near the northern border of Beijing, China (40.65°N, 117.17°E, 293.9 m a.s.l.), about 100 km northeast of the urban center (**Figure 1**). The SDZ site is a World Meteorological Organization (WMO)/Global Atmosphere Watch (GAW) background station in northern China, which has representation of air pollutants in rural NCP. The sampling site is located on the roof of the station, approximately 6 m from the ground. The prevailing wind at night and in the morning is northeasterly and turns to southwesterly in the afternoon due to effect of local valley wind. The SDZ site is upwind of the polluted NCP region, surrounded by extensive vegetation and sparsely-populated small villages. The mean $PM_{2.5}$ concentration in 2020 at the SDZ site is 26 $\mu g\ m^{-3}$, much lower than present air quality standard in China (35 $\mu g\ m^{-3}$). An integrated observation experiment was performed at the SDZ site from 10/13 to 10/27, 2020, including measurements of PAN, VOCs, O_3, HONO, NO_x, CO and photolysis rates. At the same time, we also performed PAN observations at an urban site in Beijing, located on the campus of the Minzu University of China (39.95°N, 116.32°E). The urban site is between the second and third ring roads in downtown Beijing, mainly affected by traffic and residential sources.
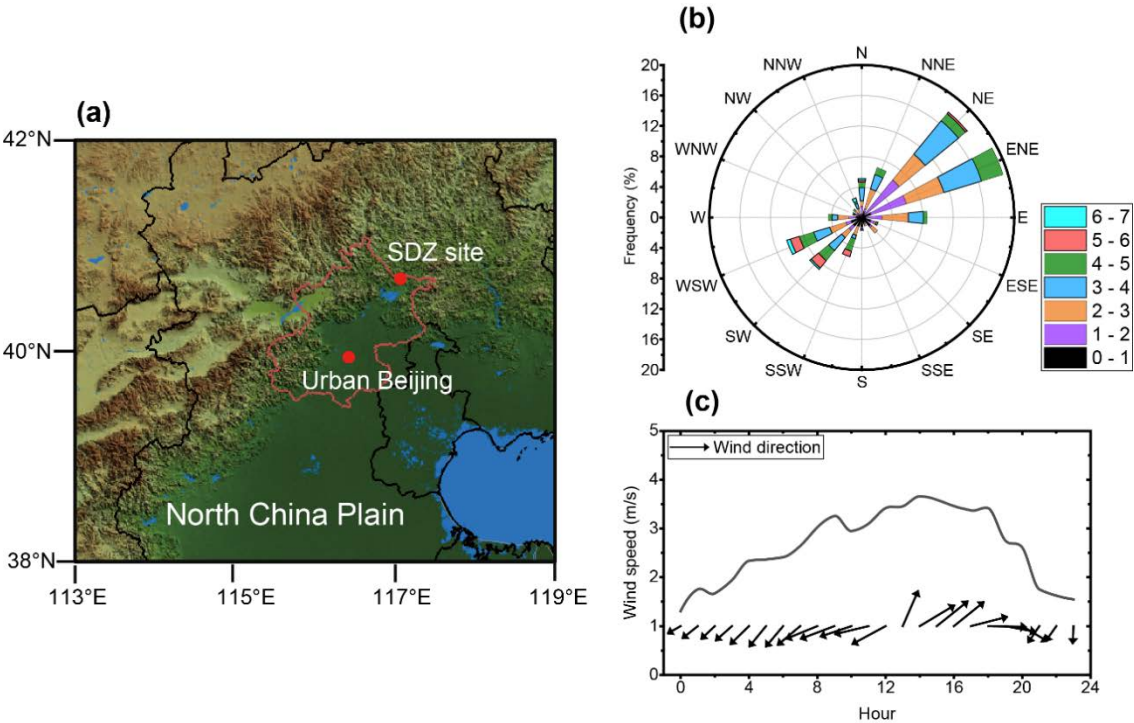
Figure 1. **(a) Locations of the SDZ site, urban Beijing and North China Plain. (b) Wind frequencies (%) and (c) diurnal wind variations averaged during the observation period at the SDZ site.**

2.2 Instruments and measurements

Details of the instruments used in this study has been summarized in **Table S1**. PAN is measured with an online gas chromatograph equipped with an electron capture detector (GC-ECD). The capillary column is mounted in a compact temperature-controlled oven whose temperature is fixed at 12°C. The ECD temperature is maintained at 50°C ± 0.2°C. The PAN instrument has a time resolution is of 5 minutes with a detection limit of 20 ppt. More information about the configuration of this instrument has been presented in our previous work (Qiu et al., 2020a). To calibrate the GC-ECD instrument, PAN is produced throughout the reactions between a calibrated NO flow (1 ppm, Linde SPECTRA Environmental Gases) and the 285-nm photolysis of excess acetone. The reaction yield of PAN is 93%. A regular multiple-point calibration check (PAN concentrations: 1ppb, 2ppb, 4ppb) has been conducted every month to guarantee the quality of PAN results since August 2015, usually on a day characterized by persistent northerly winds with low PAN concentrations.

We use the proton transfer reaction time of flight mass spectrometer (PTR-ToF-MS) to measure concentrations of formaldehyde, acetaldehyde, acetone, propene and isoprene. The ambient air is pumped into a cabin with a flow rate of 15 L min^{-1} through a 3 m long teflon tube. We use a teflon membrane fliter to remove the particles in the air flow. Then the air is envolved into a reaction drift tube of PTR-ToF-MS through 1/16 in. PEEK tubing inlet. We set the drift tube at 60°C, 2.2 mbar and 600V. H_3O^+ is used as the primary reaction ion as it has been widely used in analyzing trace gases. The measurement has a time resolution of 5 minutes. A gas calibration unit (GCU-a: GCU-advanced v2.0) is used to perform the zero air generation and PTR-ToF-MS calibration, also produced from the PTR-ToF-MS manufacturer, Ionicon. A VOC scrubber catalyst is installed in the GCU-a unit and heated at 350 °C, thus producing VOC-free zero air by passing ambient air. We use a dynamic dilution of the multicomponent gas standard (Apel Riemer Environmental Inc., USA) to calibrate the PTR-ToF-MS every month, including formaldehyde, acetaldehyde, acetone, propene and isoprene of 1 ppm ± 5%. Detailed descriptions of the PTR-ToF-MS configuration and calibration methods are listed in Sheng et al. (2018).

HONO measurements are carried out using a long-path absorption photometer (LOPAP-03, QUMA). The HONO gas is collected in the atmosphere and then absorbed by solutions. The sampling rates of gas flow and liquid flow are set to 1.3 L min^{-1} and 0.30–0.34 mL min^{-1}, respectively. We used a known concentration of nitrous acid standard solution to calibrate the LOPAP instrument every week to guarantee data quality. Besides, we also carried out zero measurements everyday lasting 1 h during the observation period.

Online measurements of O_3, NO_x, $PM_{2.5}$, and CO are also conducted using a UV photometric O_3 analyzer (model 49i, Thermo Electron Corporation, USA), a NO_x analyzer (model 42i, Thermo Electron Corporation, USA), a TEOM-1405 analyzer, and a cavity ring-down spectrometer (G2401, Picarro, Inc., USA), respectively. It is noteworthy that parts of PAN could be considered as NO_2 because of the disadvantage of model 42i analyzer. Photolysis rates (*J*), including $J_{O(^1D)}$, J_{HCHO}, and J_{HONO} are simultaneously measured by the PFS-100 Photolysis Rate Analyzer (Focused Photonics Inc., China). The analyzer receives solar radiation with a quartz probe and transfers the radiation to the spectrum via optical quartz fibers. The spectrum data is evaluated and compared with reference data via a mathematical approach to obtain the photolytic rate.

 2.3 Other data

As the SDZ site is also a national meteorology observatory, meteorological variables, including temperature (T), relative humidity (RH), sea level pressure (SLP), wind direction and speed, were continuously measured during the observation period. The hourly European Centre for Medium-Range Weather Forecasts Reanalysis v5 (ERA5) data ($0.25° \times 0.25°$), accessed from https://cds.climate.copernicus.eu/, is used to assess the impact of atmospheric circulation on

150 pollutant levels. Concentrations of odd oxygen ($O_x = O_3 + NO_2$) obtained from the Beijing Municipal Ecological and Environmental Monitoring Center (http://www.bjmemc.com.cn/) are also utilized. Here, we average the mixing ratios over 8 stations in the urban region and at the MiYunshuiku (MY) site to represent the O_x levels in urban region and rural region near SDZ, respectively.

3 Results

155 **3.1 High PAN levels during haze events in autumn**

Figure 2a shows the temporal variations in PAN and related atmospheric components at the SDZ site from 10/13 to 10/27, 2020. The mean concentrations of PAN, $PM_{2.5}$, O_3, NO_x, HCHO, HONO, CH_3CHO and C_3H_6 are 1.11 ± 0.88 ppb, 34.2 ± 23.8 μg m^{-3}, 27.6 ± 14.5 ppb, 8.5 ± 2.8 ppb, 4.9 ± 3.9 ppb, 0.15 ± 0.16 ppb, $1.6\pm.1.1$ ppb, and 0.7 ± 0.5 ppb, respectively. Compared with recent studies in China (**Table S2**), the observed PAN concentration at the SDZ site is generally lower than

160 1.5−1.89 ppb over the urban NCP (Zhang et al., 2017; Liu et al., 2018) and 2.05 ppb in urban southwestern China (Sun et al., 2020), comparable to 0.93−1.04 ppb in the suburban NCP region (Qiu et al., 2019a; Zhang et al., 2019). But it is remarkably higher than several observations from the southern China with PAN levels of 0.55−0.63 ppb (Zhu et al., 2018; Zeng et al., 2019a; Hu et al., 2020) and 0.36−0.44 ppb in Tibet (Xu et al., 2018), implying a severe photochemical pollution level over the NCP on a regional scale.
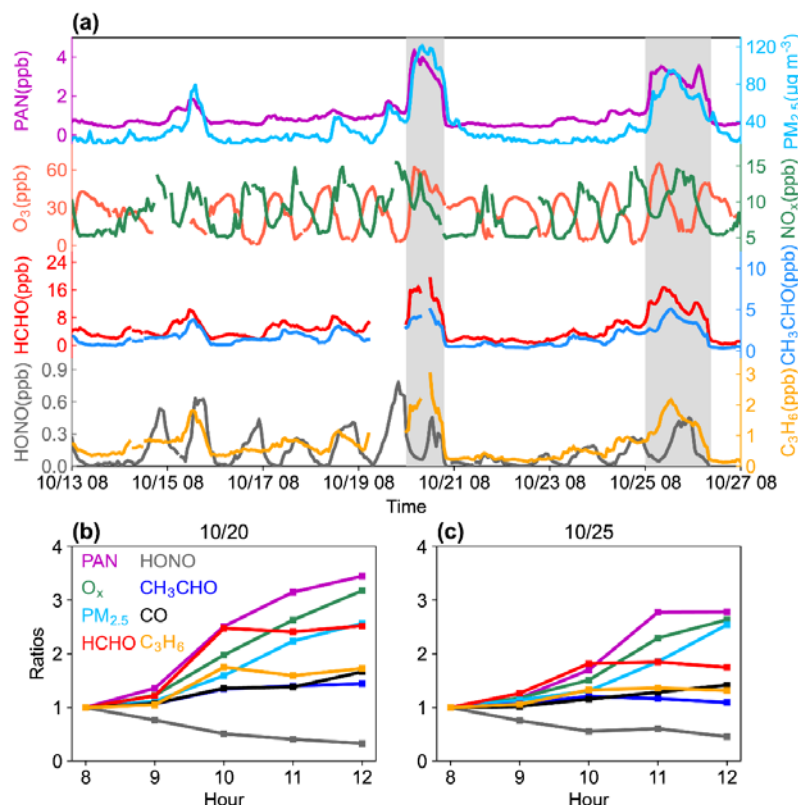
Figure 2. (a) Observed hourly concentrations of PAN (ppb), PM$_{2.5}$ (μg m^{-3}), O$_3$ (ppb), NO$_x$ (ppb), HCHO (ppb), CH$_3$CHO (ppb), HONO (ppb) and C$_3$H$_6$ (ppb) at the SDZ site from 10/13 to 10/27, 2020. The shades denote the days when hourly PAN concentrations exceed 3 ppb. (b−c) Ratios of atmospheric constituent concentrations to the concentrations at 8:00 a.m. on the mornings of 10/20 and 10/25 when substantial PAN growths take place.

As shown in **Figure 2a**, two pollution events (10/20 and 10/25–10/26) occurred at the SDZ site with hourly PAN concentrations in excess of 3 ppb. Meanwhile, daytime O$_3$ concentrations during the two pollution episodes were 16−39 % higher than those on clean days (**Table 1**). Similar increase was also found in PM$_{2.5}$, which was strongly correlated with PAN with a correlation coefficient (*R*) of 0.9 during the observation period. Daily mean NO$_x$ concentrations on pollution days were 16–42% higher than clean days as shown in **Table 1**, implying the potential role of regional transport under unfavorable meteorological conditions. Substantial increases in PAN and related pollutants could be identified on the mornings of 10/20 and 10/25. **Figure 2b-c** display the ratios of individual component concentrations to their concentrations at 8:00 a.m. on the two pollution days. In general, PAN concentrations exhibited fast growth ratios by 244% and 178% over the morning hours (8:00−12:00) of 10/20 and 10/25, which were 10.6 and 7.7 times larger than those during clean days. These increase rates are highest among all species illustrated in **Figure 2b-c.** The corresponding growth ratios of 9−44% for

PAN's primary precursor CH$_3$CHO and 41−66% for chemically inert CO are much lower than PAN. This result suggests the potential enhanced local photochemistry at the SDZ site on pollution days during autumn.

Table 1. Statistical results of concentrations for PAN (ppb), PM$_{2.5}$ (µg m^{-3}), O$_3$ (ppb), NO$_x$ (ppb), HCHO (ppb), CH$_3$CHO (ppb), C$_3$H$_6$ (ppb) and HONO (ppb) on average, during clean days and pollutions days. The clean days represent the time excluding the pollution days (10/20 and 10/25−10/26), and the daytime denotes 8:00−19:00.

Species	Mean	Clean	Pollution		
			10/20	10/25	10/26
PAN (ppb)	1.11±0.88	0.77±0.35	2.67±1.17	2.33±1.06	2.09±1.06
Daytime PAN	1.22±0.99	0.79±0.25	3.41±0.95	2.85±0.85	2.17±1.07
O$_3$ (ppb)	27.6±14.5	26.2±12.2	34.6±22.2	31.8±22.5	31.0±14.0
Daytime O$_3$	36.1±11.5	33.7±8.4	46.7±17.9	46.8±18.0	39.1±10.9
PM$_{2.5}$ (µg m^{-3})	34.2±23.8	25.7±12.9	81.5±33.2	57.2±25.7	57.2±18.5
NO$_x$ (ppb)	8.47±2.80	7.93±2.54	11.3±2.31	10.8±4.35	9.24±3.58
HCHO (ppb)	4.86±3.88	3.63±2.19	14.1±3.67	10.9±4.35	7.21±4.62
CH$_3$CHO (ppb)	1.61±1.09	1.31±0.75	3.87±0.61	3.09±1.09	2.26±1.45
C$_3$H$_6$ (ppb)	0.70±0.50	0.56±0.33	1.94±0.49	1.28±0.52	0.94±0.62
HONO (ppb)	0.15±0.16	0.13±0.14	0.34±0.25	0.17±0.09	0.25±0.17

Previous studies also reported synchronous increases of PAN and PM$_{2.5}$ during cold seasons over the NCP region (Liu et al., 2018; Zhang et al., 2019). For example, Zhang et al., (2019) showed that PAN concentration was doubled at noon during a haze episode at a suburban site in Beijing in comparison with that in the morning, along with synchronous increases of PM$_{2.5}$ and O$_3$. Liu et al. (2018) also reported rapid growth of PAN during a wintertime pollution event in urban Jinan along with high PM$_{2.5}$ concentration; however, they showed rather low O$_3$ concentration during winter haze days because of high NO$_x$ concentrations and intense NO titration effects in the urban region. Therefore, synchronous increases of PAN and PM$_{2.5}$ can take place in the whole NCP region during cold days, while co-occurrence of O$_3$ increases may just exist in suburban and background regions where NO$_x$ emissions are rather low.

3.2 Meteorological conditions

On synoptic scale, PAN levels are largely influenced by meteorological conditions. **Figure 3** shows the atmospheric circulation during clean days and two pollution days (10/20 and 10/25), focusing on variations of sea level pressure and wind in the boundary layer. During the observation period, the SDZ site was affected by a high-pressure system in the west associated with northwesterly wind in the upper boundary layer. Similar weather pattern was also identified on clean days, facilitating pollutant diffusion. During the two pollution days, southwesterly winds prevailed over the NCP. On 10/20, the SDZ site was to the south of a strong low-pressure system, leading to southwesterly winds arisen from pressure gradient

force. The southwesterly winds on 10/25 were caused by a weak high-pressure system with an anticyclone in the southeast. As the observation site is located north of the urban region, the prevailing southwesterly winds could promote pollution transport from downtown Beijing to the rural site.
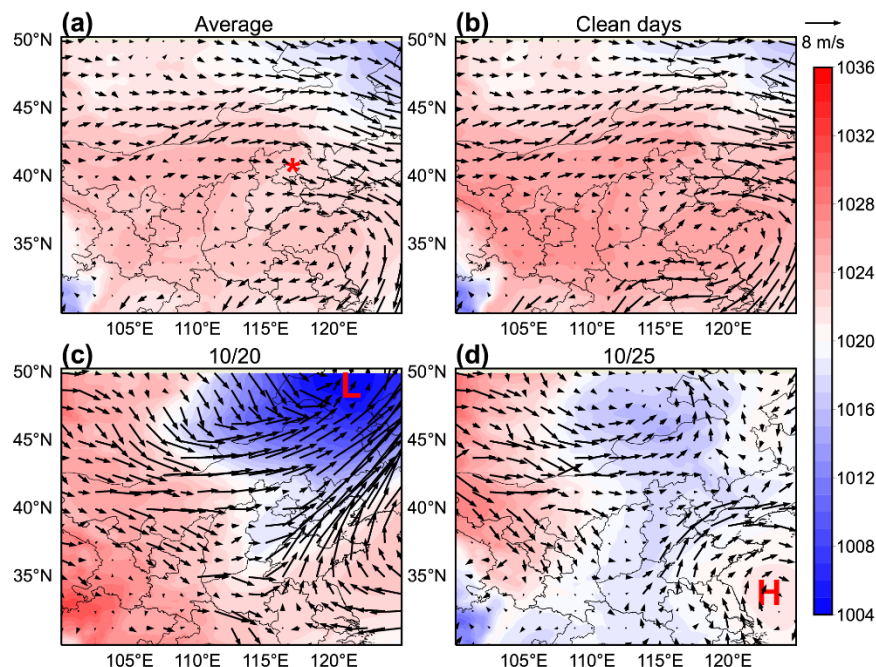
Figure 3. **Winds at 925 hPa and sea level pressure (hPa) derived from ERA5 data (a) averaged during 10/13−10/27, (b) clean days (10/13−10/19, 10/21−10/24) and on (c) 10/20 and (d) 10/25. The red asterisk in (a) shows the location of the SDZ site.**

Temporal variations of observed meteorological variables at the SDZ site are shown in **Figure 4a-e**. The daytime T, RH, SLP, $J_{O(^1D)}$ and meridional wind (V) near the surface are also compared between clean days and pollution days, illustrated as boxplots in **Figure 4f-j**. Here, positive V values denote southerly winds, while negatives represent northerly winds. We find positive daytime T and RH anomalies on 10/20 and 10/25, indicating hot and wet weather conditions compared with clean days. Although higher temperature can promote thermal decomposition of PAN, it also accelerates photochemistry thus increases PAN levels. Higher RH has been proved to inhibit heterogeneous reactions of PAN on soot, leading to increase of PAN concentration in the atmosphere (Zhao et al., 2017). Negative SLP anomalies and positive V anomalies on 10/20 and 10/25 could contribute to pollution accumulation and transport to the north, coinciding with the ERA5 results shown in **Figure 3**. As shown in **Figure 4j**, daytime $J_{O(^1D)}$ on 10/20 and 10/25 were 3.1×10^{-6} s^{-1} and 4.3×10^{-6} s^{-1}, which were 47% and 26% lower than that on clean days (5.8×10^{-6} s^{-1}). These reductions are likely to result from aerosol and cloud radiative effects, which is unfavorable for photochemical reactions. Consequently, the meteorological conditions during pollution events are favorable for accumulation and transport of PAN and its precursors, as well as promoting chemical formation due to relatively higher temperature and RH compared with clean days, though reductions of photolysis rates are identified.
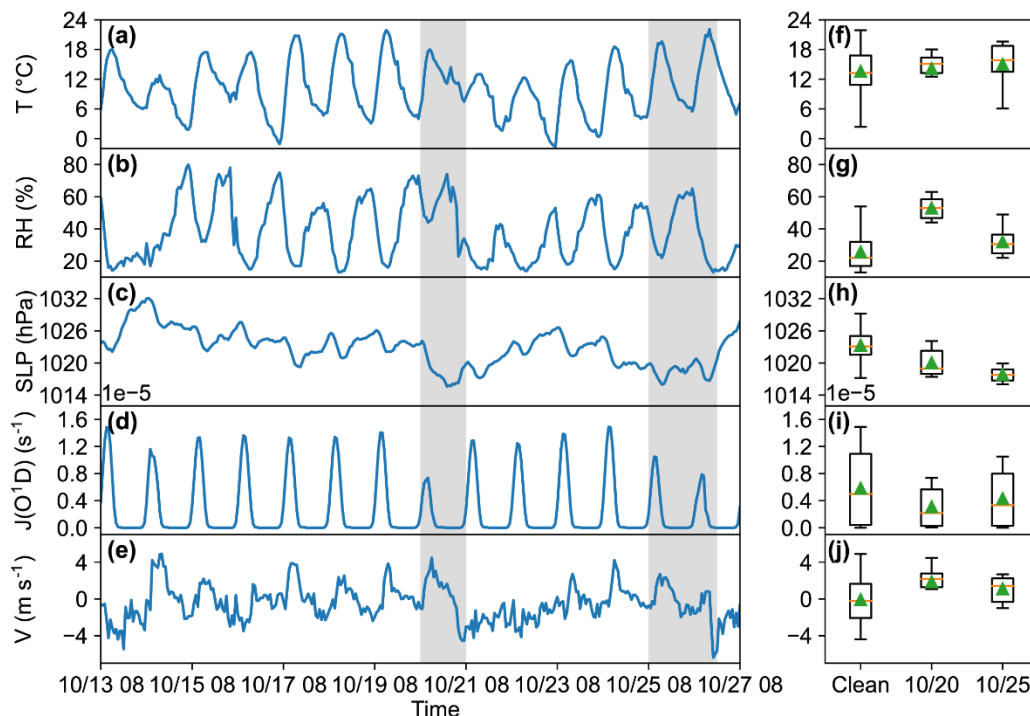
Figure 4. (a-e) Time series of observed temperature (T; ºC), relative humidity (RH; %), sea level pressure (SLP; hPa), photolysis rate for O_3 ($J_{O(^1D)}$; s^{-1}) and meridional wind (V; m s^{-1}) during 10/13−10/27 at the SDZ site. The shades denote the pollution days. **(f-j)** Box plots for daytime meteorological parameters during clean days (10/13−10/19, 10/21−10/24) and two pollution days. The red lines and green triangles denote the median and mean values, respectively.

3.3 Strong local photochemistry at the SDZ site

As the SDZ site is a clean background station with scarce anthropogenic sources, the substantial increases in PAN and other secondary pollutants on 10/20 and 10/25 were tentatively supposed in relation to pollutant transport from the urban region. However, this increases on pollution days are impossibly caused by direct PAN transport from the urban region, though its relatively long thermal lifetime during the observation period (~1 day). Here, direct PAN transport refers to PAN itself, excluding its precursors. **Figure 5a-c** show the temporal variations of daytime PAN and O_x at the urban, SDZ and MY site on the two pollution days when abrupt increases of PAN take place. Detailed locations of the three sites and distances between them are shown in **Figure 5d**. Southerly wind facilitates pollutant transport from the urban region to the SDZ site, while northerly wind brings relatively clean air. On 10/20, the PAN concentrations at the SDZ site rose from 1.3 ppb at 8:00 a.m. to 4.3 ppb at 12:00 p.m. However, the wind did not turn to southerly until 10:00 a.m. (**Figure 5a**). The calculated transport distance was just about 26 km during 10:00 a.m. to 12:00 p.m. as the observed southerly wind speed was 1.2−3.4 m/s. It is approximately the distance between the SDZ site and the MY site, another rural site near the Miyun Reservoir

240 (**Figure 5d**). The O_x concentration at the MY site during 9:00 a.m. to 12:00 p.m. of 10/20 was slightly lower than that at the SDZ site (**Figure 5c**), indicating the similar photochemical pollution levels between the two sites. Therefore, the substantial increase of PAN on the morning of 10/20 was not likely driven by direct PAN regional transport, despite the observed high PAN concentration at the urban site (**Figure 5a**). On another pollution day (10/25), the prevailing wind turned to southerly after 12:00 p.m. Direct PAN transport from the urban region could not explain the fast PAN growth in the morning. Besides,

245 PAN increases in the morning resulted from planetary boundary layer evolution are deemed to be unlikely, because our previous observation at an urban site of the NCP region has reported that nighttime PAN concentration in autumn of 2018 in upper boundary layer was just 9.5% higher than surface-layer PAN concentration (Qiu et al., 2019a). The slightly higher PAN concentration in upper layer could not be the cause of rapid increases of PAN on the mornings of pollution days.
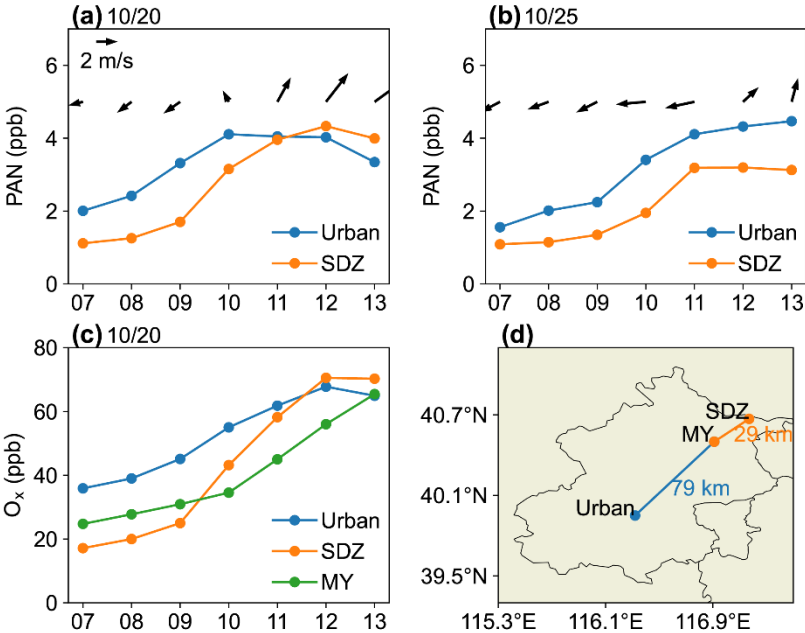
250 **Figure 5**. **Hourly variations of PAN concentrations (ppb) and surface wind at the urban and SDZ site during 7:00−13:00 on (a) 10/20 and (b) 10/25. (c) Hourly variation of O_x concentrations (ppb) at the urban, SDZ and MY site during 7:00−13:00 on 10/20. (d) Detailed locations of the urban, SDZ and MY site and the distances between them.**

As shown in **Figure 2b-c**, the increase rates of PAN during pollution days at the SDZ site are much larger than CO. It is

255 known that CO is chemically inert and served as an ideal tracer for anthropogenic sources, which can well represent transport processes from pollution sources (Gao et al., 2005; Worden et al., 2013; Chen et al., 2020). Thus, further evidence of enhanced photochemistry during the pollution episodes comes from the quantitative assessment of direct PAN transport and chemical production using CO as a tracer. Ambient PAN concentration is affected by physical processes (such as

regional transport) and local photochemical formation. Thus, the change rate of PAN at the SDZ site ($\frac{d[PAN]}{dt}$) is the sum of

260 net chemical production rate ($\frac{d[Chem]}{dt}$) and change due to physical processes ($\frac{d[Phys]}{dt}$)

$$\frac{d[PAN]}{dt} = \frac{d[Chem]}{dt} + \frac{d[Phys]}{dt} \tag{Eq.1}$$

As there are no intense anthropogenic sources along the transport from downtown Beijing to the SDZ site, we assume that PAN/CO ratios remain constant along the transport pathway and PAN change rate at the SDZ site due to direct physical transport ($\frac{d[Phys]}{dt}$) is identical with that of CO ($\frac{d[CO]}{dt}$)

265 $$\frac{d[Phys]}{dt} = \frac{d[CO]}{dt} \times \frac{[PAN]}{[CO]} \tag{Eq.2}$$

Net chemical production rate ($\frac{d[Chem]}{dt}$) is the sum of chemical production (P[PAN]) and thermal decomposition (Eq. 3). Thermal decomposition rate (L[PAN]) can be calculated as $-k$[PAN] where the chemical reaction rate coefficient k is temperature-dependent (Seinfeld and Pandis, 2006). Therefore, the chemical production of PAN (P[PAN]) can be derived from the difference between net chemical production rate ($\frac{d[Chem]}{dt}$) and chemical decomposition rate, as shown in Eq.4

270 $$\frac{d[Chem]}{dt} = P[PAN] - k[PAN] \tag{Eq.3}$$

$$P[PAN] = \frac{d[PAN]}{dt} - \frac{d[CO]}{dt} \times \frac{[PAN]}{[CO]} + k[PAN] \tag{Eq.4}$$

We use 4 hours as dt and sperate a day as morning (8:00−12:00), afternoon (12:00−16:00), evening (16:00−20:00) and night (20:00−08:00). It should be noted that the assumption of constant PAN/CO ratio along the transport pathway may lead to underestimation of physical impacts, especially in the afternoon when temperature is high. Therefore, the change rates due to 275 chemical processes calculated by PAN/CO method are maximum values that are possible.

Figure 6 displays the process diagnostic results of PAN at the SDZ site. Here, we define PAN change rates induced by chemical processes and physical processes as Chem and Phys, respectively. Positive PAN change rate (Chem + Phys) was only found in the morning (8:00−12:00), which was attributed to high net chemical production rate (Chem) of 0.14 ppb h^{-1}. In the afternoon (12:00−16:00) and evening (16:00−20:00), regional transport (Phys) by southwesterly winds contributed to 280 increases in PAN with rates of 0.05 ppb h^{-1} and 0.02 ppb h^{-1}, respectively. However, the negative net chemical production rates (−0.07 ppb h^{-1} and −0.06 ppb h^{-1}) originating from large thermal loss rates (L[PAN], −0.57 ppb h^{-1} and −0.34 ppb h^{-1}) completely overcome the PAN increases from transport. This evidence manifests local photochemical formation of PAN in the morning, coinciding with PAN's diurnal variation. The impacts of photochemistry and regional transport on PAN were both largely strengthened during pollution days (**Figure 6 and Figure S1**). The net chemical formation rate (Chem) was 0.45 285 ppb h^{-1} on the morning of pollution days, which was 6.3 times as large as that on clean days. This again demonstrates that strong local photochemical reactions contribute most to PAN enhancement on the mornings of the two pollution days, rather than direct transport.
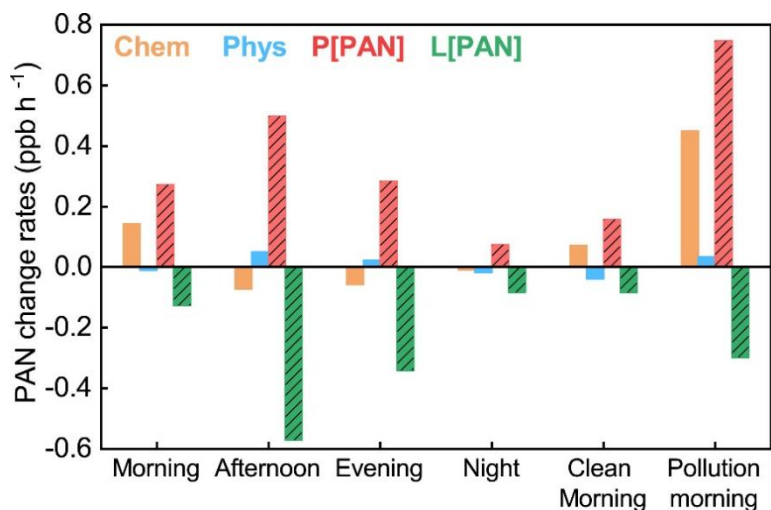
290 **Figure 6**. **Process diagnostic analysis of PAN on average and on the mornings of clean and pollution days. Chem, Phys, P[PAN], and L[PAN] denote the net chemical production, physical changes, chemical production and loss rates of PAN, respectively. Morning, afternoon, evening and night correspond to 8:00−12:00, 12:00−16:00, 16:00−20:00 and 20:00−08:00, respectively.**

3.4 Impacts of precursors on rapid increase of PAN

A key question in explaining the substantial increase of PAN at the SDZ site is how its precursors change. PAN is
295 directly formed through the reaction between PA radical and NO_2. As NO_2 is much more abundant than PAN in the
atmosphere, PA formation through VOC oxidation and photolysis may have greater impacts on PAN. As noted above, the
dominant three pathways of PA formation are through direct oxidation of CH_3CHO, photolysis of acetone and methylglyoxal
(MGLY) (Fischer et al., 2014). **Figure 7** displays the calculated PA production rates through these three VOC species. The
PA production through $CH_3CHO+OH$ is calculated by $k \times [CH_3CHO] \times [OH]$, where $k=5.55 \times 10^{-12} \times \exp(311/T)$ (Seinfeld and
300 Pandis, 2006), CH_3CHO concentration is obtained from PTR-ToF-MS measurements, while OH concentration is assumed to
be with a maximum value of 3.0×10^6 molec cm^{-3} at noon, which is consistent with Lu et al. (2019). The PA production rates
through photolysis of acetone and MGLY are calculated by $J_{acetone} \times [acetone]$ and $J_{MGLY} \times [MGLY]$, where the photolysis
rates (J) are estimated using the tropospheric ultraviolet and visible radiation (TUV) model described in Madronich and
Flocke (1999). The acetone concentration is collected from PTR-ToF -MS measurements, and the MGLY concentration is
305 obtained from Qiu et al., (2020c) in which the modified modeling MGLY concentration near the SDZ site in autumn of 2018
was about 0.012 ppb. Besides, we also calculate the contribution from oxidation of MGLY by OH to PA production using
$k \times [MGLY] \times [OH]$. As seen in **Figure 7**, CH_3CHO oxidation by OH radical plays a dominant role in PA production at the
SDZ site. The relatively lower photolysis rate of acetone ($\sim 10^{-7}$ s^{-1}) and previously reported low MGLY concentration
(~ 0.012 ppb) in autumn at the rural site (Qiu et al., 2020c) inhibit high PA production rates through these two species.
310 Although methacrolein (MACR) and methyl vinyl ketone (MVK), oxidation products of isoprene and monoterpene, also

contribute to PA production through photolysis (Liu et al., 2010; Fischer et al., 2014), the observed low concentration (average: 0.12 ppb) in autumn resulted in noontime PA production rate of about 5500 molec cm^{-3} s^{-1}. This is even lower than the PA production rate from acetone photolysis. Our results are consistent with previous studies, in which they have also confirmed the dominant role of CH$_3$CHO+OH in PA formation during winter in urban Beijing (Xu et al., 2021), over eastern China (Zeng et al., 2019a; Zhang et al., 2020b) and even on global scale (Fischer, et al., 2014).
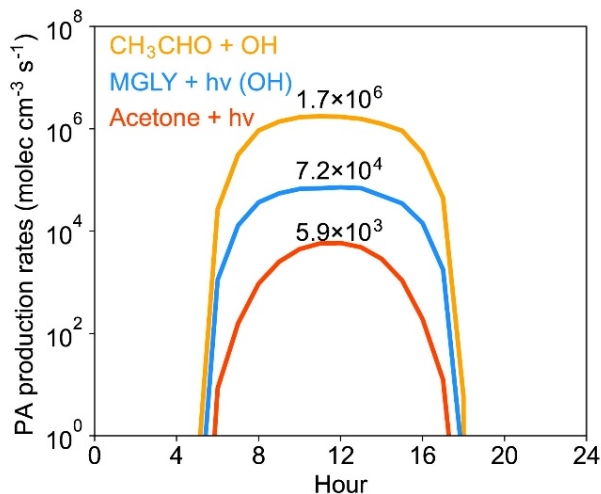
Figure 7. **Estimated variations of daytime PA production rates (molec cm^{-3} s^{-1}) through CH$_3$CHO, acetone and MGLY averaged during the observation period at the SDZ site. The numbers on the top of the lines denote the maximum values at noon through three pathways.**

The calculation of PA production rates by CH$_3$CHO and OH can also help us estimate PA concentration in suppose that PA radical can reach steady state. Thus, we can also obtain PAN production rates by the product of reaction coefficient, PA and NO$_2$ concentrations (**Method S2**). Using this method, the calculated mean PAN production rate in the morning was 0.25 ppb h^{-1}, and increased to about 0.6 ppb h^{-1} on pollution days (**Figure S2**). Although these values are slightly lower than those estimated by PAN/CO method (0.27 ppb h^{-1} and 0.73 ppb h^{-1}) shown in **Figure 6**, the comparable PAN production rates using two different methods also suggest the enhanced photochemistry during pollution days.

CH$_3$CHO could be directly emitted to the atmosphere and also formed through oxidations of alkenes, such as C$_3$H$_6$. **Figure 8** shows the daily variations of CH$_3$CHO and C$_3$H$_6$ concentrations at the SDZ site during Episode 1 (10/16−10/20) and Episode 2 (10/22−10/26). Here, we use the daily concentrations at 8:00 a.m. to represent the VOC level before daytime active photochemistry. On 10/16, the NCP region was influenced by a high-pressure system with northerly winds (**Figure 4e**), which was conducive to pollutant diffusion. From 10/17 to 10/20, persistent stagnant conditions with southerly winds during late morning to evening contributed to pollutant accumulation and transport from the urban region to the SDZ site, though northerly winds prevailed from night to morning. Thus, the C$_3$H$_6$ and CH$_3$CHO concentrations at the SDZ site during

10/16 to 10/20 both exhibited increasing trends, reflecting the cumulative effect. Similar in appearance to that from 10/22 to
10/25 (**Figure 8d-e**), during which the C_3H_6 and CH_3CHO concentrations increased by 180 % and 196 %. These indicate that cumulative effect under persistent stagnant weather conditions increased VOC concentration levels before strong photochemistry occurred on the mornings of 10/20 and 10/25. Furthermore, high PAN/NO_2 ratios on 10/20 and 10/25 when rapid increases of PAN appeared (**Figure 8c, f, i**) also enabled the identification of strong photochemistry with a relatively high precursor level. As illustrated in **Figure 6**, the net chemical formation rate on the morning of pollution days was 6.3 times larger than that on clean days. However, the increase ratios for CH_3CHO and C_3H_6 were just about 2.8 times as large as that on clean days (**Figure 8g-h**). That is to say, increases of VOC concentration could not fully explain the remarkable increase in PAN, although it indeed promoted the photochemical formation of PAN during the two pollution events.
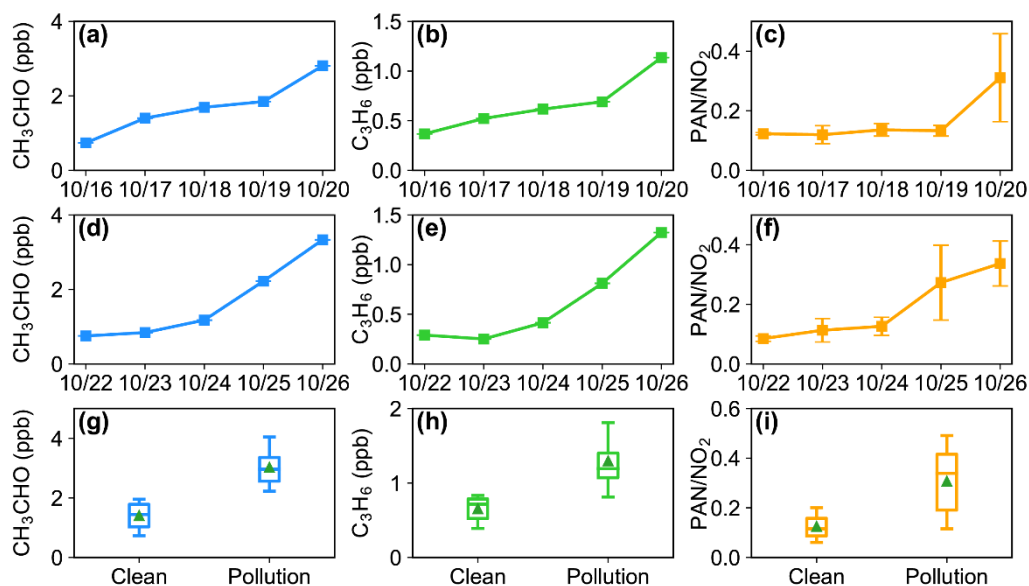
Figure 8. Observed concentrations of CH_3CHO (ppb), C_3H_6 (ppb) and PAN/NO_2 ratios at 8:00 a.m. (a-c) during Episode 1 (10/16−10/20) and (d-f) Episode 2 (10/22−10/26) at the SDZ site. Comparisons between concentrations of CH_3CHO, C_3H_6 and PAN/NO_2 ratios on the mornings of clean days (10/13−10/19, 10/21−10/24) and pollution days (10/20, 10/25−10/26).

3.5 Impacts of radicals on rapid increase of PAN

In addition to VOC precursors, the observed strengthened chemical formation on the mornings of pollution days could also relate to increased OH concentration and atmospheric oxidation capacity. Photolysis of HONO, HCHO, and O_3 can provide the major source of HO_x radicals (Schnell et al., 2009; Edwards et al., 2014; Tan et al., 2018; Li et al., 2021). Here, the calculated time series of HO_x production through photolysis of HONO, HCHO, and O_3 using comprehensive measurements over the rural NCP is shown in **Figure 9**. The calculation method has been described in **Method S2**. Unlike HONO and O_3, photolysis of HCHO directly produces HO_2. Recycling of HO_2+NO contributes to OH formation while

HO$_2$+HO$_2$ is the important sink of HO$_x$ in the troposphere. Calculated results show that the OH at the SDZ site can be immediately produced through reaction of NO+HO$_2$ as the production rate of NO+HO$_2$ is remarkably higher than HO$_2$ loss rate through HO$_2$+HO$_2$ (**Table S3**). Thus, we use HO$_x$ here to represent the OH level. On average, a maximum HO$_x$ production rate (P[HO$_x$]) of 6.5×10^6 molec cm^{-3} s^{-1} was observed at noon (**Figure 9b**). The P[HO$_x$] could be particularly large during pollutions days (**Figure 9a**). **Figure 10** compares the P[HO$_x$] during clean days and pollution episodes. The noontime P[HO$_x$] on pollution days (11.0×10^6 molec cm^{-3} s^{-1}) was approximately 2 times as large as that on clean days, implying enhanced atmospheric oxidation capacity.
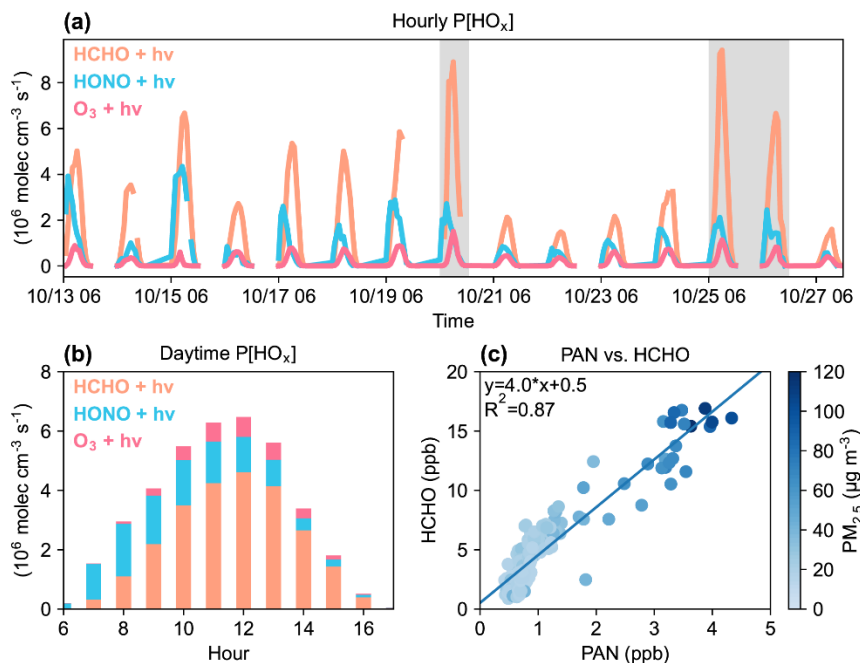
Figure 9. (a) Hourly time series of calculated HO$_x$ production rates (P[HO$_x$]) through photolysis of O$_3$, HONO and HCHO during 06:00−17:00 from 10/13 to 10/27 at the SDZ site. (b) Daytime P[HO$_x$] through each pathway averaged during 10/13 to 10/27. (c) Daytime PAN concentrations versus HCHO concentrations from 10/13 to 10/27 at the SDZ site. The colors denote the corresponding PM$_{2.5}$ levels.

In the conventional view, photolysis of HONO could provide the major source of OH radical during cold days over the NCP region (Hendrick et al., 2014; Tan et al., 2018). Here we provide the observational evidence of the dominant role of HCHO photolysis in daytime HO$_x$ productions in autumn over the rural NCP. Photolysis of HONO was vital in the early morning, but it became less important after 9:00 a.m. due to its fast decomposition with increasing sunlight (**Figure 9b**). On average, the P[HO$_x$] through HCHO photolysis reached to 4.6×10^6 molec cm^{-3} s^{-1} at noon, accounting for 71% among the three pathways (**Figure 9b**). During pollution days (10/20 and 10/25−10/26), the HCHO photolysis rate reached to 8.3×10^6 molec cm^{-3} s^{-1} at noon, which was 140% higher than that on clean days (**Figure 10**). Moreover, PAN is strongly correlated

with HCHO (R^2=0.87) (**Figure 9c**). It proves the similar source of PAN and HCHO, also demonstrates a potential impact of
375   HCHO photolysis on PAN increase at the rural site with accelerated photochemistry. The HO_x sources during cold days have
been a subject of recent interest in the field of atmospheric chemistry over the NCP region (Tan et al., 2018; Xue et al.,
2020). Using the observation-based box models, most of these studies reported the importance of HONO in OH radical and
atmospheric oxidation capacity during cold days over the NCP. By comparisons, our result at the SDZ site presents a much
lower HONO concentration (average: 0.15 ppb) than Tan et al. (2018) and Xue et al. (2020). As the SDZ site is located in
380   the north border of the NCP region, which is much cleaner than the suburban and rural site in Tan et al. (2018) and Xue et al.
(2020), thus less affected by short-live species, such as NO_x and HONO. For another, Tan et al. (2018) and Xue et al. (2020)
conducted measurements during 2016−2017 with HONO concentrations of 0.05−0.98 ppb and 1.8 ppb, while our results
were based on observations in autumn of 2020. The decrease of NO_x emissions during 2016−2020, caused by strict air
pollution control measures since 2013, could explain the observed lower HONO concentration in our study.

385
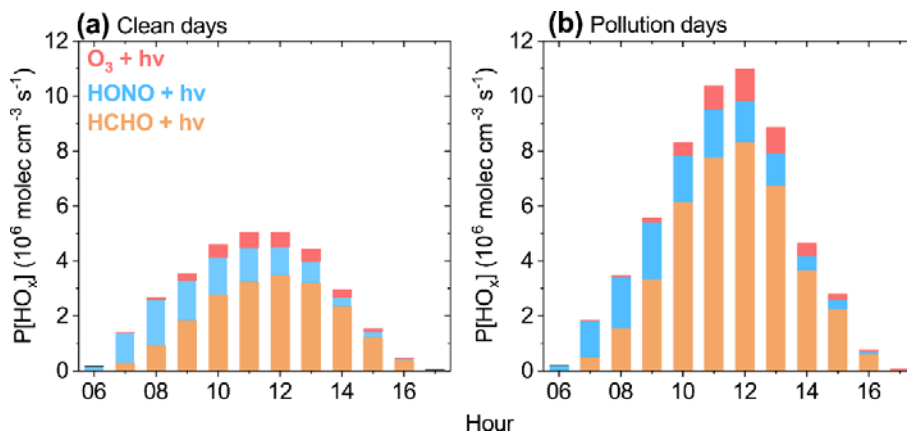
Figure 10. **Diurnal variations of P[HO_x] through three pathways during the daytime of clean days (a, 10/13−10/19, 10/21−10/24) and pollution days (b, 10/22, 10/25 and 10/26) at the SDZ site.**

390   HCHO at the SDZ site can be largely affected by aged air mass from the urban NCP region instead of biogenic source,
because the observed mean concentration of isoprene during pollution days is rather low (0.2 ppb). As shown in **Table S4**,
the observed mean HCHO concentration of 4.6±3.8 ppb at the SDZ site is lower than most observations in urban and
suburban Beijing (3.2−29.2 ppb) (Pang et al., 2009; Duan et al., 2012; Zhang et al., 2012; Rao et al., 2016; Sheng et al., 2018;
Yang et al., 2018; Qian et al., 2019; Zhou et al., 2019) and urban Guangzhou in summer (7.6 ppb) (Ling et al., 2017). But it
395   is slightly higher than observations in other southern China (2.1−5.6 ppb) (Guo et al., 2016; Wang et al., 2017; Yang et al.,
2019; Zeng et al., 2019b) and the background NCP region (3.5−3.7 ppb) conducted 3−6 years before our experiments (Yang
et al., 2017; Wang et al., 2020).

4 Discussion and implication

From the results above, we conclude that the substantial increase of PAN at the SDZ site in autumn is a result of local enhanced photochemistry from increased VOC precursor concentrations and HO_x production under a relatively warmer, wetter atmosphere and southerly wind anomalies. On the mornings of pollution days, the mean concentration of CH_3CHO is 2.8 times larger than that on clean days. This increase is due to persistent southerly winds, bringing polluted air mass from urban region to the SDZ site. Besides, the $P[HO_x]$ on pollution days is about 2 times as large as that during clean days, owing to enhanced photolysis of HCHO and HONO. The increases in CH_3CHO level and $P[HO_x]$ on pollution days could almost explain the enhanced net chemical formation rate (6.3 times of that on clean days) with nearly constant reaction rate coefficient. Accelerated photochemistry by enhanced NO_x and VOCs facilitates the rapid increase of PAN at the background site in autumn.

Unlike previous studies in which HONO was considered as the key factor of accelerating PAN formation during pollution days (Liu et al., 2018; Zhang et al., 2020b, Hu et al., 2020), our results demonstrate the dominant role of HCHO photolysis in HO_x production and PAN formation during autumn over the rural NCP region. The enhanced HCHO photolysis on pollution days not only promotes chemical production of PAN, but also accelerates formation of other secondary pollutants. This is evidenced by the synchronously increased concentrations of PAN, $PM_{2.5}$ and O_3 on pollution days, highlighting the importance of HCHO photolysis from VOC oxidation in secondary pollutant formation under low-NO_x conditions even during autumn. On the other hand, HCHO itself is also a photochemical product mainly formed through oxidation by NMHCs. Its high level during pollution days and strong correlation with PAN imply the potential role of accelerated photochemistry by enhanced NO_x and VOCs in increases of photochemical pollutants.

The importance of HCHO photolysis on secondary pollutants as we demonstrated from the SDZ site measurement could also be applicable to regions with low NO_x emissions but high reactive VOC emissions during cold seasons. The Chinese government has conducted effective NO_x emission controls since 2013 and summertime VOC emission controls in recent years. Our results show that it is also imperative to implement the VOC controls out of the summer season to avoid the unexpectedly enhanced photochemistry with decreasing NO_x emissions over the NCP region.

5 Conclusion

We performed an integrated observation experiment at a rural site in the northern border of the NCP region in autumn 2020. The observed results show rapaid increases of PAN on two pollution days with increasing ratios of 244% and 178% over the morning hours (8:00−12:00). Meteorlogical reanalysis data together with surface observations reveal that southwesterly winds prevail in the NCP during pollution days with a warmer and wetter atmosphere. However, the substantial increases of PAN on pollution days are impossibly resulted from direct PAN transport from the urban region, as the time when the prevailing wind turned to southerly is too late. Using CO as a tracer to exclude impact of physical transport of PAN from the urban region, we find that the net chemical formation rates on the morning of pollution days is

430 0.45 ppb h^{-1}, which is 6.3 times larger than that on clean days. Therefore, the strong local photochemistry could be the main cause of PAN enhancement on the morning of the two pollution days.

Further investigation reveals that CH_3CHO oxidation by OH is the major pathway of PA formation at the SDZ site. The C_3H_6 and CH_3CHO concentrations during 10/16−10/20 and 10/22−10/26 exhibit increasing trends, demonstrating the cumulative effect and regional transport from urban region under a meteorological condition of persistent southerly winds
435 during late morning to evening. Statistical results show that the mean CH_3CHO concentration on the morning of pollutions days is 2.8 times larger than that on clean days. Additionally, the P[HO_x] on pollution days was about 2 times that during clean days, owing to enhanced photolysis of HCHO and HONO despite weaker radiation at that time. Consequently, the rapid increase of PAN at the SDZ site in autumn is a result of local enhanced photochemistry from increases of VOC precursor concentrations and HO_x levels. Our study explores the cause of rapid increase of PAN concentration at a
440 background site of the NCP region, and emphasizes the important role of HCHO in secondary pollutant formation in autumn. It is vital for understanding winter photochemistry under low NO_x emissions.

Data availability

The ERA5 data is accessed from https://cds.climate.copernicus.eu/. The observation data for O_x at the MY and urban site is obtained from the Beijing Municipal Ecological and Environmental Monitoring Center (http://www.bjmemc.com.cn/). The
445 observation data used in this study can be accessed via https://doi.org/10.7910/DVN/EPAGNB.

Author contributions

YQ and ZM designed the study. YQ carried out the analysis and wrote the paper. YQ, ZM, MH, JS, PT, WP and HZ together conducted the observation experiment. KL, JZ, TH, YT and HL helped interpret the results. ZM and KL helpled revise this paper.

450 **Competing interests**

The authors declare that they have no conflict of interest.

Acknowledgements

The authors would like to thank the staff of the Shangdianzi station for their excellent work. This research was supported by the Beijing Natural Science Foundation (Grant No. 8194078), the Open fund by Jiangsu Key Laboratory of Atmospheric
455 Environment Monitoring and Pollution Control (Grant No. KHK2001) and the National Natural Science Foundation of China (Grant No. 41475135).

References

Alicke, B., Geyer, A., Hofzumahaus, A., Holland, F., Konrad, S., Pätz, H. W., Schäfer, J., Stutz, J., Volz-Thomas, A., and Platt, U.: OH formation by HONO photolysis during the BERLIOZ experiment, Journal of Geophysical Research: Atmospheres, 108, PHO 3-1-PHO 3-17, https://doi.org/10.1029/2001JD000579, 2003.

Chen, Y. J., Ma, Q. L., Lin, W. L., Xu, X. B., Yao, J., and Gao, W.: Measurement report: Long-term variations in carbon monoxide at a background station in China's Yangtze River Delta region, Atmospheric Chemistry and Physics, 20, 15969-15982, 10.5194/acp-20-15969-2020, 2020.

Dang, R., Liao, H., and Fu, Y.: Quantifying the anthropogenic and meteorological influences on summertime surface ozone in China over 2012–2017, Science of The Total Environment, 754, 142394, https://doi.org/10.1016/j.scitotenv.2020.142394, 2021.

Duan, J., Guo, S., Tan, J., Wang, S., and Chai, F.: Characteristics of atmospheric carbonyls during haze days in Beijing, China, Atmospheric Research, 114-115, 17-27, https://doi.org/10.1016/j.atmosres.2012.05.010, 2012.

Edwards, P. M., Brown, S. S., Roberts, J. M., Ahmadov, R., Banta, R. M., deGouw, J. A., Dubé, W. P., Field, R. A., Flynn, J. H., Gilman, J. B., Graus, M., Helmig, D., Koss, A., Langford, A. O., Lefer, B. L., Lerner, B. M., Li, R., Li, S.-M., McKeen, S. A., Murphy, S. M., Parrish, D. D., Senff, C. J., Soltis, J., Stutz, J., Sweeney, C., Thompson, C. R., Trainer, M. K., Tsai, C., Veres, P. R., Washenfelder, R. A., Warneke, C., Wild, R. J., Young, C. J., Yuan, B., and Zamora, R.: High winter ozone pollution from carbonyl photolysis in an oil and gas basin, Nature, 514, 351-354, 10.1038/nature13767, 2014.

Fischer, E. V., Jacob, D. J., Yantosca, R. M., Sulprizio, M. P., Millet, D. B., Mao, J., Paulot, F., Singh, H. B., Roiger, A., Ries, L., Talbot, R. W., Dzepina, K., and Deolal, S. P.: Atmospheric peroxyacetyl nitrate (PAN): a global budget and source attribution, Atmospheric Chemistry and Physics, 14, 2679-2698, 10.5194/acp-14-2679-2014, 2014.

Gao, J., Wang, T., Ding, A. J., and Liu, C. B.: Observational study of ozone and carbon monoxide at the summit of mount Tai (1534m a.s.l.) in central-eastern China, Atmospheric Environment, 39, 4779-4791, 10.1016/j.atmosenv.2005.04.030, 2005.

Guo, S., Chen, M., and Tan, J.: Seasonal and diurnal characteristics of atmospheric carbonyls in Nanning, China, Atmospheric Research, 169, 46-53, https://doi.org/10.1016/j.atmosres.2015.09.028, 2016.

Hendrick, F., Müller, J. F., Clémer, K., Wang, P., De Mazière, M., Fayt, C., Gielen, C., Hermans, C., Ma, J. Z., Pinardi, G., Stavrakou, T., Vlemmix, T., and Van Roozendael, M.: Four years of ground-based MAX-DOAS observations of HONO and NO_2 in the Beijing area, Atmos. Chem. Phys., 14, 765-781, 10.5194/acp-14-765-2014, 2014.

Heuss, J. M. and Glasson, W. A.: Hydrocarbon reactivity and eye irritation, Environmental Science & Technology, 2, 1109-1116, 1968.

Hu, B., Liu, T., Hong, Y., Xu, L., Li, M., Wu, X., Wang, H., Chen, J., and Chen, J.: Characteristics of peroxyacetyl nitrate (PAN) in a coastal city of southeastern China: Photochemical mechanism and pollution process, Science of the Total Environment, 719, 10.1016/j.scitotenv.2020.137493, 2020.

Kim, S., VandenBoer, T. C., Young, C. J., Riedel, T. P., Thornton, J. A., Swarthout, B., Sive, B., Lerner, B., Gilman, J. B., Warneke, C., Roberts, J. M., Guenther, A., Wagner, N. L., Dubé, W. P., Williams, E., and Brown, S. S.: The primary and recycling sources of OH during the NACHTT-2011 campaign: HONO as an important OH primary source in the wintertime, Journal of Geophysical Research: Atmospheres, 119, 6886-6896, https://doi.org/10.1002/2013JD019784, 2014.

Li, K., Jacob, D. J., Shen, L., Lu, X., De Smedt, I., and Liao, H.: Increases in surface ozone pollution in China from 2013 to 2019: anthropogenic and meteorological influences, Atmospheric Chemistry and Physics, 20, 11423-11433, 10.5194/acp-20-11423-2020, 2020.

Li, K., Jacob, D. J., Liao, H., Qiu, Y., Shen, L., Zhai, S., Bates, K. H., Sulprizio, M. P., Song, S., Lu, X., Zhang, Q., Zheng, B., Zhang, Y., Zhang, J., Lee, H. C., and Kuk S. K., Ozone pollution in the North China Plain spreading into the late-winter haze season, PNAS, 118, e2015797118, 2021.

Ling, Z. H., Zhao, J., Fan, S. J., and Wang, X. M.: Sources of formaldehyde and their contributions to photochemical O3 formation at an urban site in the Pearl River Delta, southern China, Chemosphere, 168, 1293-1301, https://doi.org/10.1016/j.chemosphere.2016.11.140, 2017.

Liu, L., Wang, X., Chen, J., Xue, L., Wang, W., Wen, L., Li, D., and Chen, T.: Understanding unusually high levels of peroxyacetyl nitrate (PAN) in winter in Urban Jinan, China, Journal of Environmental Sciences, 71, 249-260, https://doi.org/10.1016/j.jes.2018.05.015, 2018.

Liu, J., Liu, Z., Ma, Z., Yang, S., Yao, D., Zhao, S., Hu, B., Tang, G., Sun, J., Cheng, M., Xu, Z., and Wang, Y., Detailed budget analysis of HONO in Beijing, China: Implication on atmosphere oxidation capacity in polluted megacity, Atmospheric Environment, 244, 117957, 2021.

Liu, Z., Wang, Y., Gu, D., Zhao, C., Huey, L. G., Stickel, R., Liao, J., Shao, M., Zhu, T., Zeng, L., Liu, S.-C., Chang, C.-C., Amoroso, A., and Costabile, F.: Evidence of Reactive Aromatics As a Major Source of Peroxy Acetyl Nitrate over China, Environmental Science & Technology, 44, 7017-7022, 10.1021/es1007966, 2010.

Lu, K., Fuchs, H., Hofzumahaus, A., Tan, Z., Wang, H., Zhang, L., Schmitt, S. H., Rohrer, F., Bohn, B., Broch, S., Dong, H., Gkatzelis, G. I., Hohaus, T., Holland, F., Li, X., Liu, Y., Liu, Y., Ma, X., Novelli, A., Schlag, P., Shao, M., Wu, Y., Wu, Z., Zeng, L., Hu, M., Kiendler-Scharr, A., Wahner, A., and Zhang, Y.: Fast Photochemistry in Wintertime Haze: Consequences for Pollution Mitigation Strategies, Environmental Science & Technology, 53, 10676-10684, 10.1021/acs.est.9b02422, 2019.

Lu, X., Zhang, L., Wang, X., Gao, M., Li, K., Zhang, Y., Yue, X., and Zhang, Y.: Rapid Increases in Warm-Season Surface Ozone and Resulting Health Impact in China Since 2013, Environmental Science & Technology Letters, 7, 240-247, 10.1021/acs.estlett.0c00171, 2020.

Ma, Z., Xu, J., Quan, W., Zhang, Z., Lin, W., and Xu, X.: Significant increase of surface ozone at a rural site, north of eastern China, Atmospheric Chemistry & Physics, 16, 3969-3977, 2016.

Madronich, S., Flocke, S., The role of solar radiation in atmospheric chemistry. In: Boule, P. (Ed.), Handbook of Environmental Chemistry. Springer-Verlag, Heidelberg, pp. 1–26, 1999.

Pang, X., Mu, Y., Zhang, Y., Lee, X., and Yuan, J.: Contribution of isoprene to formaldehyde and ozone formation based on its oxidation products measurement in Beijing, China, Atmospheric Environment, 43, 2142-2147, https://doi.org/10.1016/j.atmosenv.2009.01.022, 2009.

Qian, X., Shen, H., and Chen, Z.: Characterizing summer and winter carbonyl compounds in Beijing atmosphere, Atmospheric Environment, 214, 116845, https://doi.org/10.1016/j.atmosenv.2019.116845, 2019.

Qiu, Y., Lin, W., Li, K., Chen, L., Yao, Q., Tang, Y., and Ma, Z.: Vertical characteristics of peroxyacetyl nitrate (PAN) from a 250-m tower in northern China during September 2018, Atmospheric Environment, 213, 55-63, 10.1016/j.atmosenv.2019.05.066, 2019a.

Qiu, Y., Ma, Z., and Li, K.: A modeling study of the peroxyacetyl nitrate (PAN) during a wintertime haze event in Beijing, China, Science of the Total Environment, 650, 1944-1953, 10.1016/j.scitotenv.2018.09.253, 2019b.

Qiu, Y., Ma, Z., Lin, W., Quan, W., Pu, W., Li, Y., Zhou, L., and Shi, Q.: A study of peroxyacetyl nitrate at a rural site in Beijing based on continuous observations from 2015 to 2019 and the WRF-Chem model, Frontiers of Environmental Science & Engineering, 14, 10.1007/s11783-020-1250-0, 2020a.

Qiu, Y., Ma, Z., Li, K., Lin, W., Tang, Y., Dong, F., and Liao, H.: Markedly Enhanced Levels of Peroxyacetyl Nitrate (PAN) During COVID-19 in Beijing, Geophysical Research Letters, 47, 10.1029/2020gl089623, 2020b.

Qiu, X., Wang, S., Ying, Q., Duan, L., Xing, J., Cao, J., Wu, D., Li, X., Xing, C., Yan, X., Liu, C., and Hao, J.: Importance of Wintertime Anthropogenic Glyoxal and Methylglyoxal Emissions in Beijing and Implications for Secondary Organic Aerosol Formation in Megacities, Environmental Science & Technology, 54, 11809-11817, 10.1021/acs.est.0c02822, 2020c.

Rao, Z., Chen, Z., Liang, H., Huang, L., and Huang, D.: Carbonyl compounds over urban Beijing: Concentrations on haze and non-haze days and effects on radical chemistry, Atmospheric Environment, 124, 207-216, https://doi.org/10.1016/j.atmosenv.2015.06.050, 2016.

Schnell, R. C., Oltmans, S. J., Neely, R. R., Endres, M. S., Molenar, J. V., and White, A. B.: Rapid photochemical production of ozone at high concentrations in a rural site during winter, Nature Geoscience, 2, 120-122, 2009.

Seinfeld, J. H., Pandis, S. N., Atmospheric chemistry and physics: From air pollution to climate change. John Wiley &Sons, Inc., 2006.

Sheng, J., Zhao, D., Ding, D., Li, X., Huang, M., Gao, Y., Quan, J., and Zhang, Q.: Characterizing the level, photochemical reactivity, emission, and source contribution of the volatile organic compounds based on PTR-TOF-MS during winter haze period in Beijing, China, Atmospheric Research, 212, 54-63, https://doi.org/10.1016/j.atmosres.2018.05.005, 2018.

555 Sun, M., Cui, J. n., Zhao, X., and Zhang, J.: Impacts of precursors on peroxyacetyl nitrate (PAN) and relative formation of PAN to ozone in a southwestern megacity of China, Atmospheric Environment, 231, 10.1016/j.atmosenv.2020.117542, 2020.

Tan, Z., Rohrer, F., Lu, K., Ma, X., and Zhang, Y.: Wintertime photochemistry in Beijing: Observations of ROx radical concentrations in the North China Plain during the BEST-ONE campaign, Atmospheric Chemistry and Physics, 1-33, 560 2018.

Taylor, O. C.: Importance of peroxyacetyl nitrate (PAN) as a phytotoxic air pollutant, Air Repair, 19, 347-351, 1969.

Wang, Y., Hu, B., Tang, G., Ji, D., Zhang, H., Bai, J., Wang, X., and Wang, Y.: Characteristics of ozone and its precursors in Northern China: A comparative study of three sites, Atmospheric Research, 132-133, 450-459, https://doi.org/10.1016/j.atmosres.2013.04.005, 2013.

565 Wang, C., Huang, X.-F., Han, Y., Zhu, B., and He, L.-Y.: Sources and Potential Photochemical Roles of Formaldehyde in an Urban Atmosphere in South China, Journal of Geophysical Research: Atmospheres, 122, 11,934-911,947, https://doi.org/10.1002/2017JD027266, 2017.

Wang, J., Sun, S., Zhang, C., Xue, C., Liu, P., Zhang, C., Mu, Y., Wu, H., Wang, D., Chen, H., and Chen, J.: The pollution levels, variation characteristics, sources and implications of atmospheric carbonyls in a typical rural area of North China 570 Plain during winter, Journal of Environmental Sciences, 95, 256-265, https://doi.org/10.1016/j.jes.2020.05.003, 2020.

Wei, W., Zang, J., Wang, X., and Cheng, S.: Peroxyacetyl nitrate (PAN) in the border of Beijing, Tianjin and Hebei of China: Concentration, source apportionment and photochemical pollution assessment, Atmospheric Research, 246, 10.1016/j.atmosres.2020.105106, 2020.

Worden, H. M., Deeter, M. N., Frankenberg, C., George, M., Nichitiu, F., Worden, J., Aben, I., Bowman, K. W., Clerbaux, 575 C., Coheur, P. F., de Laat, A. T. J., Detweiler, R., Drummond, J. R., Edwards, D. P., Gille, J. C., Hurtmans, D., Luo, M., Martinez-Alonso, S., Massie, S., Pfister, G., and Warner, J. X.: Decadal record of satellite carbon monoxide observations, Atmospheric Chemistry and Physics, 13, 837-850, 10.5194/acp-13-837-2013, 2013.

Xu, W., Zhang, G., Wang, Y., Tong, S., Ma, Z., Lin, W., Kuang, Y., and Xu, X.: Aerosol Promotes Peroxyacetyl Nitrate Formation During Winter in the North China Plain, Environmental Science & Technology, 55,6,3568-3581, 580 https://doi.org/10.1021/acs.est.0c08157, 2021.

Xu, X. B., Zhang, H. L., Lin, W. L., Wang, Y., Xu, W. Y., and Jia, S. H.: First simultaneous measurements of peroxyacetyl nitrate (PAN) and ozone at Nam Co in the central Tibetan Plateau: impacts from the PBL evolution and transport processes, Atmospheric Chemistry and Physics, 18, 5199-5217, 10.5194/acp-18-5199-2018, 2018.

Xue, C., Zhang, C., Ye, C., Liu, P., Catoire, V., Krysztofiak, G., Chen, H., Ren, Y., Zhao, X., Wang, J., Zhang, F., Zhang, C., 585 Zhang, J., An, J., Wang, T., Chen, J., Kleffmann, J., Mellouki, A., and Mu, Y.: HONO Budget and Its Role in Nitrate Formation in the Rural North China Plain, Environmental Science & Technology, 54, 11048-11057, 10.1021/acs.est.0c01832, 2020.

Xue, L., Wang, T., Wang, X., Blake, D. R., Gao, J., Nie, W., Gao, R., Gao, X., Xu, Z., Ding, A., Huang, Y., Lee, S., Chen, Y., Wang, S., Chai, F., Zhang, Q., and Wang, W.: On the use of an explicit chemical mechanism to dissect peroxy acetyl nitrate formation, Environmental Pollution, 195, 39-47, 10.1016/j.envpol.2014.08.005, 2014.

Yang, X., Xue, L., Yao, L., Li, Q., Wen, L., Zhu, Y., Chen, T., Wang, X., Yang, L., Wang, T., Lee, S., Chen, J., and Wang, W.: Carbonyl compounds at Mount Tai in the North China Plain: Characteristics, sources, and effects on ozone formation, Atmospheric Research, 196, 53-61, https://doi.org/10.1016/j.atmosres.2017.06.005, 2017.

Yang, X., Xue, L., Wang, T., Wang, X., Gao, J., Lee, S., Blake, D. R., Chai, F., and Wang, W.: Observations and Explicit Modeling of Summertime Carbonyl Formation in Beijing: Identification of Key Precursor Species and Their Impact on Atmospheric Oxidation Chemistry, Journal of Geophysical Research: Atmospheres, 123, 1426-1440, https://doi.org/10.1002/2017JD027403, 2018.

Yang, Z., Cheng, H. R., Wang, Z. W., Peng, J., Zhu, J. X., Lyu, X. P., and Guo, H.: Chemical characteristics of atmospheric carbonyl compounds and source identification of formaldehyde in Wuhan, Central China, Atmospheric Research, 228, 95-106, https://doi.org/10.1016/j.atmosres.2019.05.020, 2019.

Zeng, L., Fan, G.-J., Lyu, X., Guo, H., Wang, J.-L., and Yao, D.: Atmospheric fate of peroxyacetyl nitrate in suburban Hong Kong and its impact on local ozone pollution, Environmental Pollution, 252, 1910-1919, https://doi.org/10.1016/j.envpol.2019.06.004, 2019a.

Zeng, P., Lyu, X., Guo, H., Cheng, H., Wang, Z., Liu, X., and Zhang, W.: Spatial variation of sources and photochemistry of formaldehyde in Wuhan, Central China, Atmospheric Environment, 214, 116826, https://doi.org/10.1016/j.atmosenv.2019.116826, 2019b.

Zhai, S., Jacob, D. J., Wang, X., Shen, L., Li, K., Zhang, Y., Gui, K., Zhao, T., and Liao, H.: Fine particulate matter (PM2.5) trends in China, 2013–2018: separating contributions from anthropogenic emissions and meteorology, Atmos. Chem. Phys., 19, 11031-11041, https://doi.org/10.5194/acp-19-11031-2019, 2019.

Zhang, Y., Mu, Y., Liu, J., and Mellouki, A.: Levels, sources and health risks of carbonyls and BTEX in the ambient air of Beijing, China, Journal of Environmental Sciences, 24, 124-130, https://doi.org/10.1016/S1001-0742(11)60735-3, 2012.

Zhang, H., Xu, X., Lin, W., and Wang, Y.: Wintertime peroxyacetyl nitrate (PAN) in the megacity Beijing: Role of photochemical and meteorological processes, Journal of Environmental Sciences, 26, 83-96, 10.1016/s1001-0742(13)60384-8, 2014.

Zhang, G., Mu, Y., Zhou, L., Zhang, C., Zhang, Y., Liu, J., Fang, S., and Yao, B.: Summertime distributions of peroxyacetyl nitrate (PAN) and peroxypropionyl nitrate (PPN) in Beijing: Understanding the sources and major sink of PAN, Atmospheric Environment, 103, 289-296, 10.1016/j.atmosenv.2014.12.035, 2015.

Zhang, B., Zhao, B., Zuo, P., Zhi, H., and Zhang, J.: Ambient peroxyacyl nitrate concentration and regional transportation in Beijing, Atmospheric Environment, S1352231017305022, 2017.

Zhang, B., Zhao, X., and Zhang, J.: Characteristics of peroxyacetyl nitrate pollution during a 2015 winter haze episode in Beijing, Environmental Pollution, 244, 379-387, 10.1016/j.envpol.2018.10.078, 2019.

Zhang, G., Xia, L., Zang, K., Xu, W., Zhang, F., Liang, L., Yao, B., Lin, W., and Mu, Y.: The abundance and inter-relationship of atmospheric peroxyacetyl nitrate (PAN), peroxypropionyl nitrate (PPN), O-3, and NOy during the wintertime in Beijing, China, Science of the Total Environment, 718, 10.1016/j.scitotenv.2020.137388, 2020a.

625 Zhang, J., Guo, Y., Qu, Y., Chen, Y., Yu, R., Xue, C., Yang, R., Zhang, Q., Liu, X., Mu, Y., Wang, J., Ye, C., Zhao, H., Sun, Q., Wang, Z., and An, J.: Effect of potential HONO sources on peroxyacetyl nitrate (PAN) formation in eastern China in winter, Journal of Environmental Sciences, 94, 81-87, 10.1016/j.jes.2020.03.039, 2020b.

Zhao, X., Gao, T., and Zhang, J.: Heterogeneous reaction of peroxyacetyl nitrate (PAN) on soot, Chemosphere, 177, 339-346, https://doi.org/10.1016/j.chemosphere.2017.03.001, 2017.

630 Zhou, X., Tan, J., Qin, J., Hu, J., Duan, J., and Chen, R.: Impact of emissions controls on ambient carbonyls during the Asia-Pacific Economic Cooperation summit in Beijing, China, Environmental Science and Pollution Research, 26, 11875-11887, 10.1007/s11356-019-04577-5, 2019.

Zhu, H., Gao, T., and Zhang, J.: Wintertime characteristic of peroxyacetyl nitrate in the Chengyu district of southwestern China, Environmental Science and Pollution Research, 25, 23143-23156, 10.1007/s11356-018-2412-5, 2018.

635